Proceedings of the ASME 2010 3rd Joint US-European Fluids Engineering Summer Meeting and 8th International Conference on Nanochannels, Microchannels, and Minichannels
FEDSM-ICNMM2010
August 1-5, 2010, Montreal, Canada

FEDSM-ICNMM2010-30872

NUMERICAL SIMULATION OF THERMOMAGNETIC CONVECTION IN AN ENCLOSURE USING THE LATTICE BOLTZMANN METHOD

Mahshid Hadavand
University of New Brunswick
Fredericton, New Brunswick, Canada

Aydin Nabovati
University of Toronto
Toronto, Ontario, Canada

Antonio CM Sousa
University of New Brunswick
Fredericton, New Brunswick, Canada

ABSTRACT
The application of the single relaxation time lattice Boltzmann method (LBM) is extended to the study of thermomagnetic convection in a differentially heated square cavity with an infinitely long third dimension. The magnetic field is created and controlled by placing a dipole at the bottom of the enclosure. The magnitude of the magnetic force acting on the ferrofluid is controlled by changing the electrical current through the dipole. In this study, the effects of combined natural convection and magnetic convection, which is commonly known as "thermomagnetic convection", are analysed in what concerns the flow modes and heat transfer characteristics of a magnetic fluid (ferrofluid). This is a situation of considerable interest for cooling micro-electronic devices, when natural convection does not meet the cooling requirements, and forced convection is not viable due to the difficulties associated with pumping a ferrofluid.

INTRODUCTION
Flow and heat transfer characteristics of natural convection of a magnetic fluid are of interest in many branches of science and engineering. A theory for the boundary layer regime of free convective flow in a vertical rectangular cavity with vertical wall at different temperatures and adiabatic top and bottom walls was developed by Gill [1]. Finlayson [2] first explained in 1970 how an external magnetic field imposed on a ferrofluid with varying magnetic susceptibility, *e.g.*, due to a temperature gradient, results in a non-uniform magnetic body force, which leads to thermomagnetic convection. Thermomagnetic convection is a viable approach to enhance free convection for small length scale applications, which, due to its complex nature, remains to be fully characterized. A thorough understanding of the relation between an applied magnetic field and the resulting heat transfer is necessary for the proper design and control of thermomagnetic devices [3].

The numerical studies of heat transfer with magnetic fluids reported in the literature are relatively scarce and invariably use as governing equations the Navier-Stokes and energy equations. In what follows, relevant work in the field is succinctly reviewed. Yamaguchi *et al.* [4] experimentally and numerically studied the heat transfer characteristics and flow behaviour for natural convection of a magnetic fluid in a rectangular cavity under an imposed vertical uniform magnetic field. Krakov and Nikiforov [5] determined the influence of the angle between the direction of the temperature gradient and that of a uniform magnetic field on the convection structure and intensity of heat flux by in a square cavity. Ganguly *et al.* [3] reported on the effect of temperature on the magnetic susceptibility; because they used a very strong non-uniform magnetic field, the buoyancy is neglected in their simulation. They found that the average Nusselt number on the wall increases with increasing the magnetic dipole strength and temperature but decreases by increasing the fluid viscosity.

Colloidal suspensions containing magnetic nano-particles in appropriate carrier liquids present strong magnetic dipoles, which can be influenced by external magnetic fields [6]. Typically, the suspended nano-particles have an average diameter of about 10 nm, and these colloidal suspensions are commonly known as nanofluids. When the suspended particles

have ferromagnetic properties, the suspension is referred to as a ferrofluid [7]. The solid magnetic nano-particles are covered with a dispersant material in order to keep the particles separated; therefore, preventing agglomeration of the particles due to gravity or an external magnetic field.

In the absence of an external magnetic field, the nano-particles are oriented randomly; once the external magnetic field is applied, the nano-particles align with the applied magnetic field. The generated force between the magnetic field and the homogenously distributed magnetic nano-particles enables the manipulation of the ferrofluid by adjusting the applied external magnetic field. This uniformly distributed magnetic force manifests itself as a body force analogous to the gravity field. These suspensions, in general, exhibit normal liquid behaviour coupled with super paramagnetic properties. This leads to the possibility of controlling the properties and the flow of these liquids with relatively moderate magnetic field strengths. This magnetic control has enabled numerous developments dealing with technical and medical applications, and these suspensions are already being considered the next generation heat transfer fluids as they offer the possibility of achieving heat transfer rates much higher than those of conventional heat transfer fluids and fluids containing micro-sized metallic particles [8].

In the present work, the objective is to numerically study the effects of combined natural convection and magnetic convection in a square enclosure using the lattice Boltzmann method. The square enclosure is under the influence of an imposed two-dimensional magnetic field that conforms to Maxwell's equations.

PHYSICAL MODEL

Figure 1 presents a schematic of the cavity of height D with constant, but different, temperatures on the vertical walls, which is used for the numerical simulation. The third dimension is considered to be infinite; therefore, the flow in this configuration can be assumed to be two-dimensional. The left and right vertical walls are at constant high temperature, T_h, and constant low temperature, T_c, respectively. The upper and lower walls are adiabatic. A line dipole, which provides the external magnetic field, is placed adjacent to the lower adiabatic wall at a distance d.

We assumed the ferrofluid to be electrically non-conducting, so that there is no electromagnetic free current in the flow. In addition to this assumption, we neglect stray electric field effects in the ferrofluid and we consider the magnetic field variation caused by the temperature gradients within the fluid to be negligible as compared to the magnetic field gradient itself [9]. Furthermore, we make the simplification of treating the ferrofluids as soft magnetic material, *i.e*., the ferrofluid attains the saturation magnetization easily at relatively low magnetic field intensities, but loses the magnetization rapidly once the external magnetic field diminishes. Therefore, ferrofluids, in a magnetic field, are taken as a homogeneous magnetic liquid, which moves towards regions of highest flux.

The magnetic field conforms to the Maxwell's relations in static forms [10], as follows:

$$\nabla . B = 0 \tag{1}$$

$$\nabla \times H = 0 \tag{2}$$

where B is the magnetic field inside the ferrofluid due to the line dipole which can be expressed as [3]:

$$B = \mu_0 (1+\chi) m \left[\frac{\sin\theta}{r^2} e_r - \frac{\sin\theta}{r^2} e_\theta \right] \tag{3}$$

where H and B are related through the following equation:

$$H = \frac{1}{\mu_0 (1+\chi)} B \tag{4}$$

where μ_0 is the magnetic permeability of free space, $\mu_0 = 4\pi \times 10^{-7}$ (N/A^2); m denotes the magnetic dipole moment of the electromagnet coil (having two parallel counter-conductors separated by a distance b and carrying current I) per unit length ($m = Ib/2\pi$). χ is the magnetic fluid susceptibility which, in this study is considered to have a constant value, because the temperature differences are sufficiently small to allow changes in the susceptibility to be neglected.

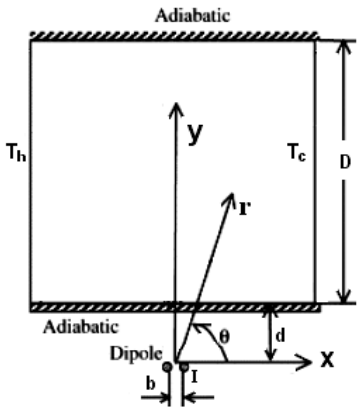

Fig. 1. Schematic of the cavity and position of the line dipole magnet.

The magnetization of the ferrofluid occurs, when it becomes polarized in the presence of an external magnetic field. Consequently, attractive forces acting on each particle are produced due to the interaction of the ferrofluid polarization and the external magnetic field. The attractive force acting on the particles can be then treated as a body force acting on the ferrofluid, which is dealt with as a homogenous medium. The attractive force on the ferrofluid per unit volume is:

$$F = (M.\nabla)B \tag{5}$$

where M is the magnetization vector and is related to H in the form of $M = \chi H$. The magnetic field strength diminishes with increasing distance from the dipole.

In this work, the single relaxation time lattice Boltzmann method is used to simulate the thermomagnetic convection in a two-dimensional square enclosure. For this particular study, only the *y*-component of the magnetic force will be considered.

NUMERICAL MODEL

The lattice Boltzmann method (LBM) is a discrete particle-based mesoscopic approach for viscous fluid flow simulation. The LBM has been shown to be an efficient tool for flow simulation in complex geometries, when compared with conventional fluid dynamics approaches [11]. In this method, finite volumes of fluid are presented as discrete particles and the fluid dynamics is obtained based on a probability distribution function of the particles and a discrete set of prescribed velocities.

Generally, there are three types of thermal lattice Boltzmann models proposed in the literature, namely: multi-speed model of McNamara and Alder [12], passive scalar model of Shan [13], and double distribution function (DDF) model of He *et al.* [14]. Among these models, the DDF model is reported to be the most stable and is the most widely used model in thermal simulations using the LBM; therefore, in the present study, the DDF thermal LBM is used.

Using the LBGK collision operator [15], the single relaxation time lattice Boltzmann equation (LBE) can be written as follows:

$$f_i(x + c_i\delta t, t + \delta t) - f_i(x,t) = -\frac{\delta t}{\tau}\left[f_i(x,t) - f_i^{eq}(x,t)\right] + f_g + F \tag{6}$$

$$g_i(\vec{x} + c_i\delta t, t + \delta t) - g_i(\vec{x},t) = -\frac{\delta t}{\tau_c}\left[g_i(\vec{x},t) - g_i^{eq}(\vec{x},t)\right] \tag{7}$$

where δt and δx are the lattice grid spacing and the lattice time step, respectively. These two are related to each other through the streaming speed, c, as $c = \delta x/\delta t$. However, in most of the LBM simulations on a uniform lattice, including the present work, δx and δt, for simplicity are considered to be equal to one. τ_v and τ_c are the momentum and internal energy relaxation times, respectively. f_g is the buoyant body force term, which is formulated by using the Boussinesq approximation [16], namely:

$$f_g = 3\omega_i\beta\rho g_y(T - T_{ave})c_{iy} \tag{8}$$

where β is the thermal expansion coefficient, g_y is the acceleration of gravity acting in the *y*-direction of the lattice links, and c_{iy} is the *y*-component of c_i. The terms ρ and T are the local density and temperature, are calculated at each lattice site. T_{ave} is the average temperature of hot and cold wall. F is the Kelvin body force, which is the force that a magnetic fluid experiences in non-uniform magnetic field that can be calculated based on equation (5).

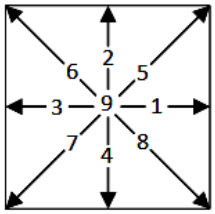

Fig. 3. Topology of the D2Q9 lattice and labelling of the directions.

The most common two-dimensional lattice is the D2Q9 lattice, which is used in this study, where '2' denotes the number of space dimensions and '9' refers to the discrete set of nine velocities as proposed by Qian *et al.* [17]. The D2Q9 lattice and its labelling for the lattice directions are shown in Fig. 3. For the D2Q9 lattice, the discrete velocity set is formulated as follows:

$$\begin{aligned} c_i &= c\left[\cos\left(\frac{(i-1)\pi}{2}\right), \sin\left(\frac{(i-1)\pi}{2}\right)\right] && i = 1,2,3,4 \\ c_i &= \sqrt{2}c\left[\cos\left(\frac{(2i-1)\pi}{4}\right), \sin\left(\frac{(2i-1)\pi}{4}\right)\right] && i = 5,6,7,8 \\ c_9 &= 0 \end{aligned} \tag{9}$$

f_i^{eq} and g_i^{eq} are the corresponding equilibrium distribution functions for the density and internal energy density distribution functions, respectively. These two parameters are in the form of a second order truncated expansion of the Maxwell-Boltzmann equilibrium function:

$$f_i^{eq} = \rho\omega_i\left[1 + \frac{1}{c_s^2}c_i.u + \frac{1}{2c_s^4}(c_i.u)^2 - \frac{1}{2c_s^2}u.u\right] \tag{10}$$

$$g_i^{eq} = \omega_i T\left[1 + \frac{1}{c_s^2}c_i.u + \frac{1}{2c_s^4}(c_i.u)^2 - \frac{1}{2c_s^2}u.u\right] \tag{11}$$

where c_s is the lattice sound speed and is equal to $1/\sqrt{3}$ for a two-dimensional lattice with 9 velocities (D2Q9). ω_i is the weighting factor and is defined as follows for the D2Q9 lattice:

$$\omega_i = \begin{cases} 4/9 & i = 9 \\ 1/9 & i = 1,2,3,4 \\ 1/36 & i = 5,6,7,8 \end{cases} \tag{11}$$

The macroscopic density and velocity on each lattice site are calculated using the distribution function on that site and the neighbouring sites as follows:

$$\rho = \sum_i f_i \tag{12}$$

$$\rho u = \sum_i c_i f_i \tag{13}$$

$$T = \sum_i g_i \tag{14}$$

The kinematic viscosity and the thermal diffusivity are given by:

$$\upsilon = \left(\tau_v - \frac{1}{2}\right) c_s^2 \tag{15}$$

$$\alpha = \left(\tau_c - \frac{1}{2}\right) c_s^2 \tag{16}$$

The no-slip solid-wall boundary condition is set for the vertical and horizontal walls of the enclosure by using the bounce back method. As mentioned before, the top and bottom walls are adiabatic, and the vertical walls are isothermal, with the right wall at higher temperature than that of the left wall.

RESULTS AND DISCUSSION

The solutions were obtained in a square two-dimensional computational domain. The parameters *D* and *d,* shown in Fig. 1, were both set to 10 mm, The density and dynamic viscosity of the ferrofluid were set equal to 1400 kg/m^3 and 1.2×10^{-2} kg/ms, respectively. Prandtl number, *Pr*, and fluid compressibility, *β,* were set equal to 5 and 2.06×10^{-4} K^{-1}, respectively.

A uniform lattice system is employed for the simulations. The numerical solution should be independent of the lattice size, and to this purpose, three different lattice sizes of 81×81, 101×101, and 121×121 were examined; results with a lattice density of 101×101 lattice units were found to be adequate to establish lattice-independent solutions for the range of the parameters used in the present study. In order to validate the thermal LBM predictions, laminar natural convection of air, *Pr* = 0.71, in a cavity was simulated for Raleigh numbers of 10^4 and 10^5. In the limiting case of no magnetic field, the predicted results with the 101×101 grid system for *Ra* = 10^4 and 10^5 were in excellent agreement with the benchmark steady flow patterns and temperature fields reported by de Vahl Davis [18]. Figures 3 and 4 show the normalized isotherms and streamlines of the convective flow in the cavity, respectively for *Ra* = 10^4 and 10^5. The general trends coincide with those reported by de Vahl Davis [18]. In Table 1, the predicted average Nusselt numbers on the hot wall are compared against values available in the literature for the same conditions, which are in excellent agreement [18]. The average Nusselt number on the side walls is determined from the following relation:

$$\overline{Nu} = -\frac{1}{\Delta T}\sum_1^D \frac{dT}{dx} \tag{17}$$

The two dimensionless parameters, the Raleigh number (*Ra*) and the Prandtl number (*Pr*), which characterize the natural convective flow, are defined as follows:

$$Ra = \frac{g_y \beta \Delta T\, D^3}{\nu\alpha} \tag{18}$$

$$\mathrm{Pr} = \frac{\nu}{\alpha} \tag{19}$$

where g_y, β, ΔT , and D are the gravitational acceleration, working fluid thermal expansion coefficient, temperature difference between the two vertical walls, and the characteristic length (equal to the width of the cavity), respectively.

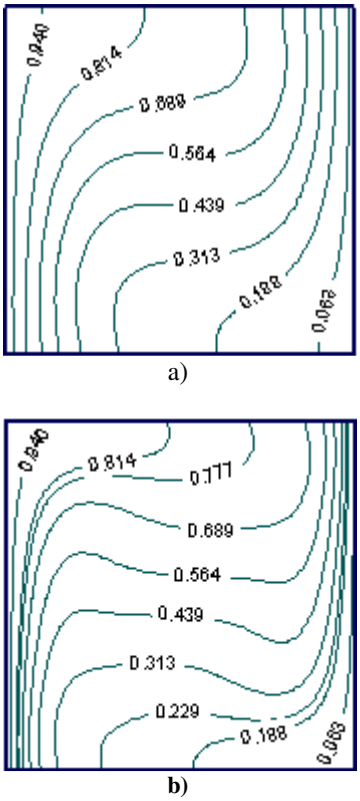

Fig. 3. Isotherms for the convective flow in the square cavity, (a) Ra=104 and Pr=0.71; (b) Ra=105 and Pr=0.71.

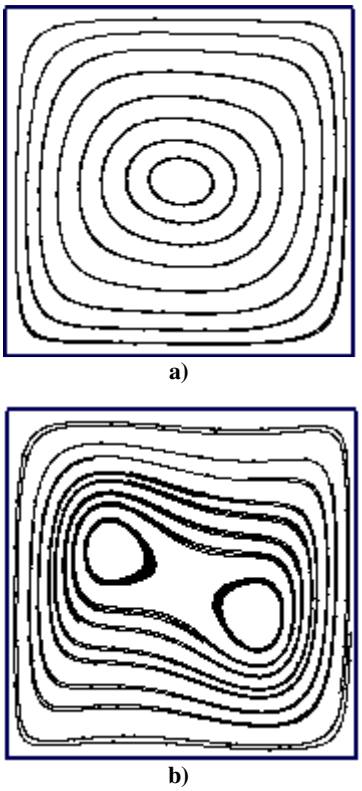

Fig. 4. Streamlines for the convective flow in the square cavity, (a) Ra=10^4 and Pr=0.71; (b) Ra=10^5 and Pr=0.71.

Table 1. Comparison of the predicted average Nusselt number for two different Raleigh numbers against the values reported in [18].

Raleigh number	Average Nusselt number	
10^4	Present work	2.249
	de Vahl Davis [18]	2.243
10^5	Present work	4.481
	de Vahl Davis [18]	4.519

The activation of the magnetic dipole will disturb the flow motion in the cavity; consequently, the temperature distribution will be affected along with the heat transfer rate at the walls of the cavity. The isotherms for four different values of m equal to 0.1, 0.3, 1, 3Am, are shown in Figs. 5a-d for Ra=10^3. The influence of the induced magnetic field on the temperature distributions is apparent. If the magnetic field magnitude is relatively weak, the buoyancy effect is dominant and the isotherms and streamlines are similar to those of pure natural convection in the absence of a magnetic field. For a stronger magnetic field, m = 1 Am, the isotherm stratification in the core diminishes, as shown in Fig. 5c; this is due to the suppression of the free convective flow by the magnetic field. By increasing the magnetic field strength, the effect of the natural convection is eventually eliminated and the flow motion of the ferrofluid is governed by the strength of the magnetic field. It should be noted that, for very strong magnetic fields, the single relaxation time LBM tend to experience numerical stability problems; consequently, only relatively moderate magnetic fields were simulated in the present study.

Figures 6a-d report the isotherms at Ra = 10^4 for m = 0.1, 0.3, 1, and 3Am. From these figures, we observe that for large values of Raleigh number, the effect of increasing m on the temperature distribution in the enclosure is less prominent compared to that in the case of a small Ra (Ra = 10^3, Fig. 5). For the case of m=1Am, the buoyancy effect still is strong enough to overcome the effect of the magnetic field. However, for sufficiently large m values, the magnetic convection is suppressed and the magnetic field effect is the dominant player. As a result, the magnetic field is the major player and the isotherms will be almost identical to the isotherms of lower Ra number case with the same relatively high magnetic field magnitude.

The streamlines for the thermomagnetic flow in the square cavity for Ra=10^3 and 10^4 and for different values of m, 0.1, 0.3, 1, and 3Am, are presented in Figs. 7a-d and 8a-d, respectively.

Table 2 summarizes the predicted values of the average Nusselt number on the hot wall for three different Raleigh numbers of 10^3, 5×10^3, and 10^4. For each Raleigh number, five different magnetic dipole strengths of m = 0, 0.1, 0.3, 1.0, and 3.0 Am were simulated.

Table 2. The predicted average Nusselt number for different Raleigh numbers and a range of magnetic dipole strengths.

Raleigh number (Ra)	Magnetic dipole strengths, m(Am)	Average Nusselt number (Nu)
10^3	0	1.116
5×10^3	0	1.761
10^4	0	2.214
10^3	0.1	1.117
5×10^3	0.1	1.759
10^4	0.1	2.211
10^3	0.3	1.128
5×10^3	0.3	1.752
10^4	0.3	2.205
10^3	1	1.664
5×10^3	1	1.850
10^4	1	2.175
10^3	3	4.786
5×10^3	3	4.708
10^4	3	4.613

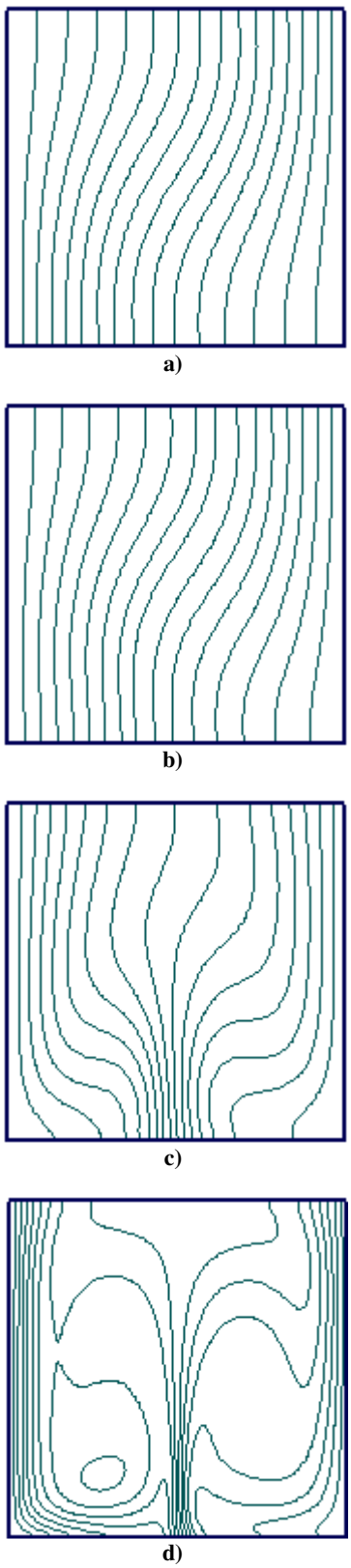

Fig. 5. Isotherms for the thermomagnetic flow in a square cavity for Ra=10^3; a) m=0.1Am, b) m=0.3Am, c) m=1Am and d) m=3Am.

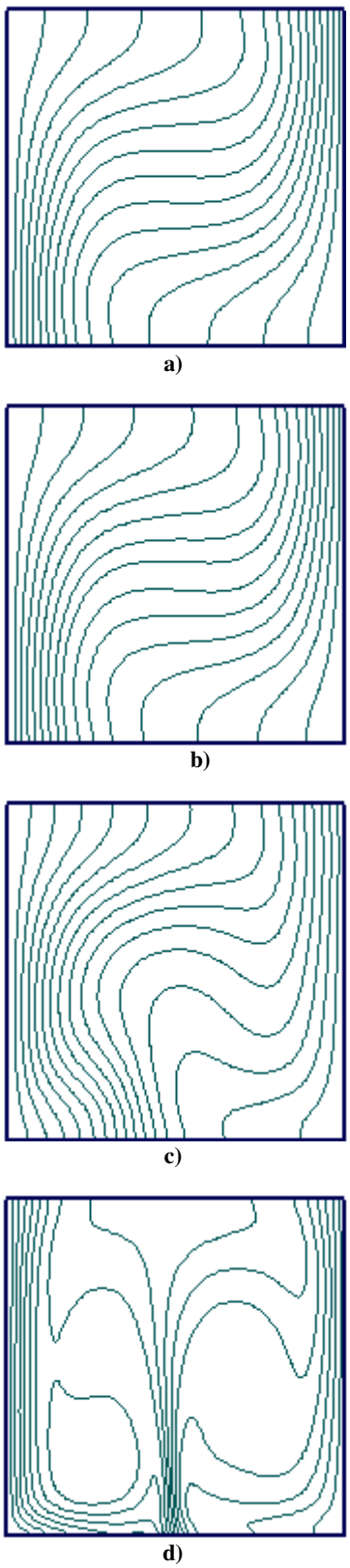

Fig. 6. Isotherms for the thermomagnetic flow in a square cavity for Ra=10^3; a) m=0.1Am, b) m=0.3Am, c) m=1Am and d) m=3Am.

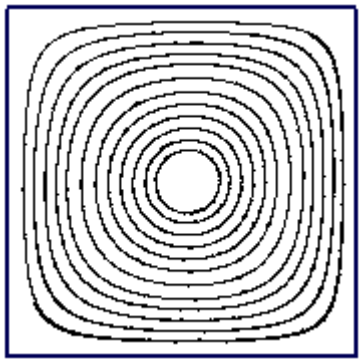

a)

b)

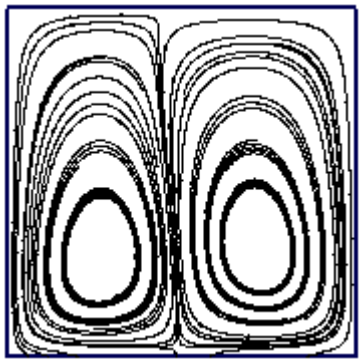

c)

d)

Fig. 7. Streamlines for the thermomagnetic flow in a square cavity for Ra=10^3; a) m=0.1Am, b) m=0.3Am, c) m=1Am and d) m=3Am.

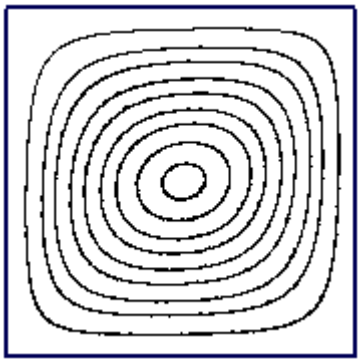

a)

b)

b)

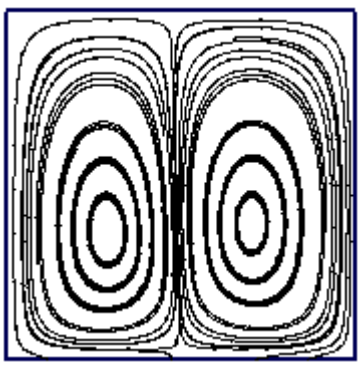

c)

Fig. 8. Streamlines for the thermomagnetic flow in a square cavity for Ra=10^3; a) m=0.1Am, b) m=0.3Am, c) m=1Am and d) m=3Am.

It can be observed that the average Nusselt number decreases by increasing m in the low range of the magnetic field, but it increases when m is increased for higher values of the magnetic field. In order to enhance the Nusselt number, the magnetic field should be strong enough to overcome the buoyant motion; as expected, for higher Raleigh numbers the magnetic field should be increased. For very high magnetic fields, the Nusselt numbers for all the Raleigh numbers tested present negligible differences. In these conditions, the buoyant force has a nearly negligible effect on the Nusselt number.

It should be reiterated the present study has not considered the variation of the magnetic susceptibility with the temperature. The inclusion of this modeling refinement would have increased the complexity of the resulting flows, as this variation would cause enhanced rotational motion of the ferrofluid. In these circumstances, the colder fluid close to the lower temperature wall moves down towards the region of larger field strength due to its higher magnetic susceptibility, while the warmer fluid with lower susceptibility is displaced away from the line dipole and is pushed upward along the hot wall. In this study, the temperature difference between the hot and cold walls is kept relatively low; consequently, the variation of the susceptibility is negligible. Preliminary calculations, where the variation was considered, have corroborated the validity of the simplification.

CONCLUSION

Simulations for thermomagnetic convection were conducted for a range of Raleigh numbers and magnetic field strengths in the laminar regime. The effects of these parameters on the heat transfer characteristics were analyzed; the numerical results showed that with the application of an external magnetic field, the temperature and velocity fields were significantly modified.

For weak magnetic fields, the average Nusselt number decreases with the increasing the magnetic field strength. However, for sufficiently high magnetic field strength, the magnetic convection is suppressed for all the examined values of the Raleigh number. For the range of the Raleigh numbers tested, the increase of the magnetic field strength does not yield a monotonic variation of the Nusselt number; in fact, the Nusselt number may increase or decrease depending on the relative strengths of the buoyancy and magnetic forces.

ACKNOWLEDGMENTS

The authors acknowledge the support received from NSERC (Natural Sciences and Engineering Research Council of Canada) Discovery Grant 12875 (ACMS).

NOMENCLATURE

c_i	particle discrete velocity set
c_s	speed of sound
d	distance between dipole and enclosure
D	enclosure height
f	distribution function for the flow field
g	distribution function for the temperature field
g_y	acceleration of gravity in the y-direction
H	defined in Eq. 4
m	magnetic field moment
M	magnetization
Nu	Nusselt number
Pr	Prandtl number
Ra	Raleigh number
t	time
T	temperature
x, y	Cartesian coordinate
u	velocity component

Greek letters

α	thermal diffusivity
β	fluid compressibility
γ	arctangent function parameter
χ	magnetic susceptibility
μ	viscosity
μ_0	magnetic permeability
ρ	density
τ	lattice relaxation time
υ	fluid kinematic viscosity
ω_i	lattice weighting factor

REFERENCES

[1] Gill, A.E., 1966, The boundary-layer regime for convection in a rectangular cavity, Journal of Fluid Mechanics, **26**, pp. 515- 536.

[2] Finlayson, B.A., 1970, Convective instability of ferromagnetic fluids, Journal of Fluid Mechanics, **40**, pp. 753-767.

[3] Ganguly, R., Sen, S. and Puri, I.K., 2004, Heat transfer augmentation using a magnetic fluid under the influence of a line dipole, Journal of Magnetism and Magnetic Materials, **271**, pp. 63–73.

[4] Yamaguchi, H., Kobori, I., Uehata, Y. and Shimada, K., 1999, Natural convection of magnetic fluid in a rectangular box, Journal of Magnetism and Magnetic Materials **201**, pp. 264–267.

[5] Krakov M.S. and Nikiforov, I.V., 2002, To the influence of uniform magnetic field on thermomagnetic convection in

square cavity, Journal of Magnetism and Magnetic Materials, **252**(1-3), pp. 209-211.

[6] Odenbach, S., 2004, Recent Progress in Magnetic Fluid Research, Journal of Physics Condensed Matter, **16**(32), pp. R1135-R1150.

[7] Raj, K. and Moskowitz, R., 1990, Commercial Applications of Ferrofluids, Journal of Magnetism and Magnetic Materials, **85**(1-3), pp. 233-245.

[8] Wang, X.-Q., and Mujumdar, A.S., 2007, Heat Transfer Characteristics of Nanofluids: A Review, International Journal of Thermal Sciences, **46**(1), pp. 1-19.

[9] Tynjälä, T., Hajiloo, A., Polashenski Jr. W. and Zamankhan, P., 2002, Magnetodissipation in ferrofluids, Journal of Magnetism and Magnetic Materials, **252**, pp. 123–125.

[10] Griffiths, D.J., 2002, Introduction to Electrodynamics, 3rd ed., Prentice Hall Inc..

[11] Nabovati, A., 2009, Pore Level Simulation of Single and Two Phase Flow in Porous Media using Lattice Boltzmann Method, PhD Dissertation, University of New Brunswick, Fredericton, New Brunswick.

[12] McNamara, G. and Alder, B., 1993. Analysis of the Lattice Boltzmann Treatment of Hydrodynamics, Physica A, **194**, pp. 218-228.

[13] Shan X., Simulation of Raleigh-Bénard convection using a lattice Boltzmann method, Physical Review E, **55**, 1997, 2780-2788.

[14] He, X., Chen, S. and Doolen, G., 1998. A Novel Thermal Model for the Lattice Boltzmann Method in Incompressible Limit, Journal of Computational Physics, **146**, pp. 282-300.

[15] Bhatnagar, P.L., Gross, E.P., and Krook, M., 1954, A model for collision process in gases. I. Small amplitude processes in charged and neutral one-component system, Physical Review, **94**, pp. 511-525.

[16] Kao, P.H. and Yang, R.J., 2008, Simulating oscillatory flows in Raleigh–Bénard convection using the lattice Boltzmann method, International Journal of Heat and Mass Transfer, **50** , pp. 3315–3328.

[17] Qian, Y.H., d'Humieres, D. and Lallemand, P., 1992, Lattice BGK model for Navier–Stokes equation, Europhysics Letters,**17**(6), pp. 479–484.

[18] de Vahl Davis, G., 1983, Natural convection of air in a square cavity: A benchmark numerical solution, International Journal for Numerical Methods in Fluids, **3**, pp. 249-264.